Electrochemical impedance spectroscopy investigation on battery materials using a symmetrical cell

Guillaume Portalis, Estelle Carrapa, Bernard Simon, Vincent Vivier

Electrochemical Impedance Spectroscopy Investigation on Battery Materials Using a Symmetrical Cell

Guillaume Portalis,[1,2] Estelle Carrapa,[1] Bernard Simon,[1] Vincent Vivier[2,*]

[1.] SAFT, Direction de la Recherche, 111-113 Bd. Alfred Daney, 33074 Bordeaux – France

[2.] Sorbonne Université, CNRS, Laboratoire Interfaces et Systèmes Electrochimiques – Paris, France

Abstract

Various works have been carried out on lithium-ion batteries for improving the different conductivities of electrode materials. For this purpose, electrochemical impedance spectroscopy is a technique of choice to understand the elementary processes that take place during the charge/discharge steps and to quantify their respective contribution in total impedance. However, some materials, such as lithium iron phosphate (LFP), suffer from poor electronic conductivity and a high interfacial resistance when used with a standard aluminum current collector. In this article, the influence of both temperature and pressure on the LFP impedance response is reported in order to provide an accurate description of the interface and a detailed analysis of the time-constants observed on the impedance response. This was made possible through the use of a carbon-coated Al current collector to decrease the contact impedance, and the development of a four-electrode symmetrical coin cell setup that allows the insertion mechanism to be studied as a function of the state of charge on a single battery, *i.e.* without the need to build a symmetrical battery for each SOC to be studied.

* corresponding author: vincent.vivier@sorbonne-universite.fr

1. Introduction

Among all materials used as positive electrodes in Li-ion batteries, lithium iron phosphate (LiFePO$_4$ – LFP) is an excellent candidate for transportation applications such as hybrid electric vehicles. Indeed, both its high thermal and good chemical stabilities meet the safety needs for the batteries used in such applications [1-3]. Moreover, its raw materials are abundant, low cost and more environmentally friendly than most other positive electrode materials [4]. However, despite these qualities, LFP not only suffers from poor intrinsic electronic and ionic conductivities [5], but also from iron dissolution [6-10] in the electrolyte and subsequent migration/diffusion of the resulting ferrous ions towards the negative electrode, the so-called « cross-talking » phenomenon. These ions are then incorporated in the solid electrolyte interphase (SEI) of graphite particles, degrading its protective properties [11, 12].

Electrochemical impedance spectroscopy (EIS) is a well-adapted technique for analyzing the different contributions to charge/discharge mechanisms as a function of frequency. In particular, the lithium ion batteries (LIBs) community have been struggling to attribute the different time-constants of the impedance spectra of the LFP to their corresponding phenomena. Some authors suggest that the predominant capacitive time constant observed in the high frequency domain should be attributed to the electrode/electrolyte interfacial resistance that contributes to the charge transfer resistance [10, 13, 14]. However, Gaberscek et al. [15] showed that changing the nature of the current collector has a great impact on this high-frequency capacitive loop. In that case, it is assumed that the use of a proper substrate material to deposit the LFP battery material ink strongly improves the quality of the ohmic contact at the interface by reducing the interfacial specific area impedance [9], and it results in a significant decrease of this impedance contribution on the total impedance response. Hence, the observed predominant time-constant of the LFP is clearly attributed to the LFP material/current collector contact. The measured impedance therefore corresponds to the sum of the impedances of the two identical electrodes in series, at the same state of charge, which can be tuned. Interestingly, with such a setup, no reference electrode is thus required.

Moreover, symmetric coin cells are usually preferred to 3-electrode configuration (*i.e.,* with reference electrode) because of artifacts that can arise due to electrochemical and geometric asymmetries [16, 17]. On the one hand, the use of a reference electrodes allows a fine monitoring of the anode potential for avoiding Li metal deposition [18]. On the other hand, it has been shown that the presence of a reference electrode may lead to heterogeneous response of the electrode beneath the reference electrode [19, 20], and may also results in artifacts in the impedance spectra of the battery [21, 22]. In the case of a symmetrical cell, the main drawbacks originate in the inability to change the SOC *in situ* and the need to dismantle the button cells, collect the electrodes

and place them in another coin cell, which considerably increases the uncertainties and handling errors [16, 23]. This is the reason why, in this work, a new 4-electrode symmetrical coin cell setup has been devised, allowing impedance measurement of electrode at different SOC to be made in symmetric configuration within one single coin cell (without the need to reconfigure the battery), cancelling the previous limitation. In particular, such an approach makes it possible to carry out a complete ageing study of the battery on the same coin-cell while avoiding damage problems (such as short circuits) by reconditioning two asymmetric batteries into a single symmetric one as is currently done. The resulting impedance is thus

In this work, a first part is dedicated to the characterization of the LFP electrode/collector contact through conventional symmetrical coin cells. Then the contact is improved by using a specifically coated current collector in order to characterize the kinetics at the LFP particles. In a second part, the use of a new 4-electrode setup with the improved current collector, which allows monitoring the state of charge within the same coin cell allows a detailed investigation of the coin-cell.

2. Experimental

2.1. Systems and electrochemical cells

The classical symmetrical coin cells are CR2425-type cells which involve two opposite LFP electrodes with two separators between them. A stainless-steel spring was welded to a 20 mm diameter stainless-steel disk to maintain and to distribute the pressure on the LFP electrodes. The pressure conditions were thus reproducible from one-coin stack to another.

All battery components, except the electrodes, were rinsed and washed with acetone (99.5% purity, Scharlau), dimethylcarbonate (DMC, 99% purity, ACROS organics) and ethanol (96% purity, Xilab) before assembling the battery. After drying of components, the coin cells were then assembled in a glove box in an argon atmosphere.

The new 4-electrode symmetrical cell, which allows EIS measurement at different SOC, is depicted in Figure 1a. It consisted of a CR2425-type cell in which LFP rings with an outer diameter of 16 mm and an inner diameter of 10 mm were replacing the usual plain LFP disks commonly used in coin-cells. The rings were directly connected to the potentiostat by a current collector wrapped in a polypropylene film and jammed between the joint ring and the lower cap. Pure lithium disks of 10 mm in diameter were placed behind each LFP ring and separated by 2 layers of separator. Lithium metal was used to allow cycling and the control of the SOC of the LFP electrodes. Such a cell geometry with drilled LFP electrodes allows the Li transport from one Li disk to the opposite LFP electrode that had its coated side facing it, and conversely, for the opposite process to happen. By connecting the lithium electrodes together and connecting the annular LFP electrodes together the system behaves as a conventional LIB as shown in Figure 1b, in which Li #1 exchanges Li ions

with LFP #2 and Li #2 exchanges Li ions with LFP #1. In other words, the SOC can be controlled and successive EIS measurements can be performed simply by changing the connection of the cell.
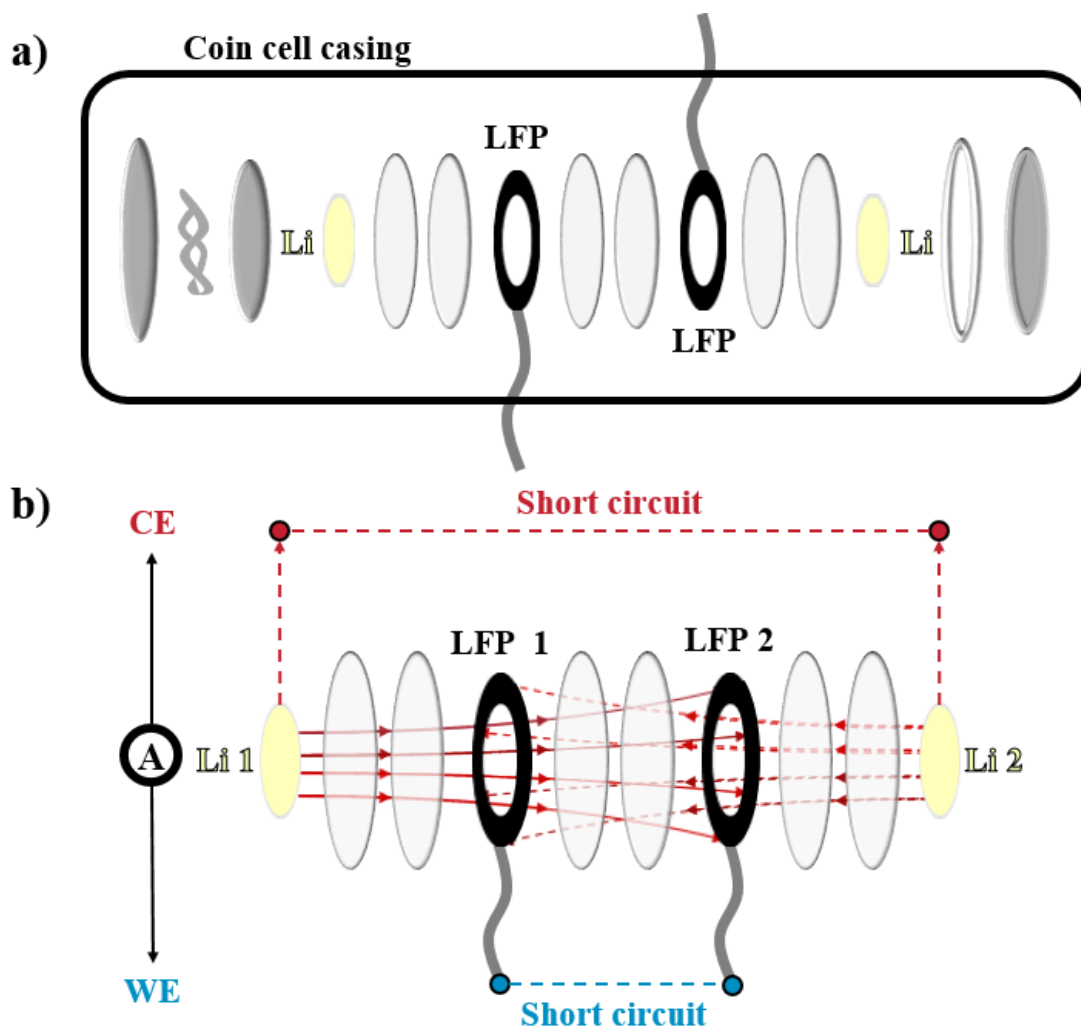
Figure 1 – Sketches of the 4-electrode symmetrical coin cell set-up devised for this study (a) and the simultaneous charge/discharge of LFP symmetrical configuration for state of charge screening (b).

2.2. Materials

The separators were stamped disks from Celgard 2325 tri-layered PP/PE/PP strips of 22 mm in diameter and 25 μm thick.

The electrolyte was a mixture of organic carbonates EC/PC/DMC/EMC (10/20/45/25 vol. %), with the adjunction of 1 wt.% of vinylene carbonate and 3 wt.% of fluoroethylene carbonate as additives, and 1 M of $LiPF_6$ as Li salt.

The electrodes consisted of a 15 μm thick aluminum foil coated on one side with the cathode material which was a blend of carbon coated LFP and $LiNi_{0.8}Co_{0.15}Al_{0.05}O_2$ (NCA) active material (90/10 wt.%) mixed with a carbon black and a binder (91/4/5 wt.%). The electrodes were coated from N-Methyl-2-pyrrolidone (NMP) based ink onto the aluminum current collector and were

dried in an oven at 90 °C for 30 min. Two thicknesses with different loadings were studied in this work: a loading of 15.6 mg cm^{-2} and a loading of 19.6 mg cm^{-2}, corresponding to an active material thickness of 70 and 86 μm, and a porosity of 33% and 32%, respectively. The electrodes were then cut to form 18 mm in diameter discs and were used in conventional symmetrical coin cells.

A second series of electrodes with the same nominal composition was single-side coated with a 10 mg cm^{-2} loading on a 17 μm thick carbon coated aluminum current collector to improve the quality of the contact between the material and the collector. Additionally, the electrodes were stamped rings with an outer diameter of 16 mm and an inner diameter of 10 mm, and were used in the new 4-electrode symmetrical coin cell setup developed in this work.

The negative electrodes used in half-coin cells for the formation steps of the LFP protective layer and the control of the SOC in the conventional symmetrical systems were Li metal disks of 18 mm in diameter and 200 μm thick.

2.3. Methods

The electrochemical tests were performed with a multi-channel MPG-2 potentiostat (BioLogic Science Instruments) and with a multi-channel VMP-3 potentiostat (BioLogic Science Instruments) for running charge/discharge cycles and for performing EIS measurements at different SOCs, respectively. The cycling procedure consisted of charge/discharge cycles at C/10 (*i.e.* 10 hours to fully charge or discharge the LFP) at different regulated temperature. The LFP/Li half cells were cycled between 2.9 V and 4.1 V, whether the system was the conventional coin-cell or the 4-electrode symmetrical cell.

Potentiostatic EIS measurements were performed in the range 100 kHz - 10 mHz with an AC voltage amplitude of 20 mV$_{p-p}$ at different SOCs. For EIS measurements in the new symmetrical configuration, the switch from cycling to EIS implies disconnecting the Li electrodes and setting the two facing LFP electrodes in a symmetric configuration.

The temperature control during both the charge/discharge cycles and the EIS measurements were performed by a Memmert and a Secasi thermal chambers for all cycles performed at 60 °C and when the temperature was varied from -20 °C to 60 °C, respectively. After any temperature change and before the acquisition of new EIS spectra, the cells are left at rest potential for 20 minutes in order to reach the steady-state.

EIS fitting was performed with a homemade software (SIMAD) in order to extract parameters of different phenomena taking place in the LIB. This software relies on the simplex method and the weighting procedure is based on the modulus of the impedance. It allows the fitting of experimental data using electrical equivalent circuits, analytical expression of the impedance or a

combination of both. All the fits performed were characterized by a χ coefficient between 0.5 and 1.5.

3. Results and discussion

3.1. LFP/collector contact

Figure 2 shows the EIS spectra performed at different temperatures from -20 to 60 °C measured for a SOC of 50%. For loading of 15.6 mg cm^{-2} (Figure 2a), one capacitive loop at 510 Hz is well defined for all temperatures, and shows a resistance that varies from 161 Ω cm^2 at -20 °C down to 102 Ω cm^2 when the temperature is increased up to 60 °C. The same qualitative observation can be made for a loading of 19.6 mg cm^{-2} (Figure 2b). Interestingly, when an additional external pressure is applied to the coin cell and thus on the LFP electrodes, the impedance values significantly decrease. Indeed, for normal pressure condition, the resistance ranges between 350 Ω cm^2 at 60 °C and 570 Ω cm^2 at -20 °C, whereas when an additional pressure is applied, these values are reduced to 78 Ω cm^2 and 130 Ω cm^2 at 60 and -20 °C (Figure 2b), respectively, reaching even lower values than with lower loading (Figure 2a). This observation is consistent with the fact that the phenomenon driving the impedance in this frequency domain has to be attributed to the electrode/collector contact: higher pressure presumably improves this contact. The contact resistance is thus an electronic contribution (pressure dependent) but there is also probably an ionic contribution in the variation of the time constant (temperature dependent) which, to our best of knowledge, remains to be explained and has not been discussed yet in the literature.
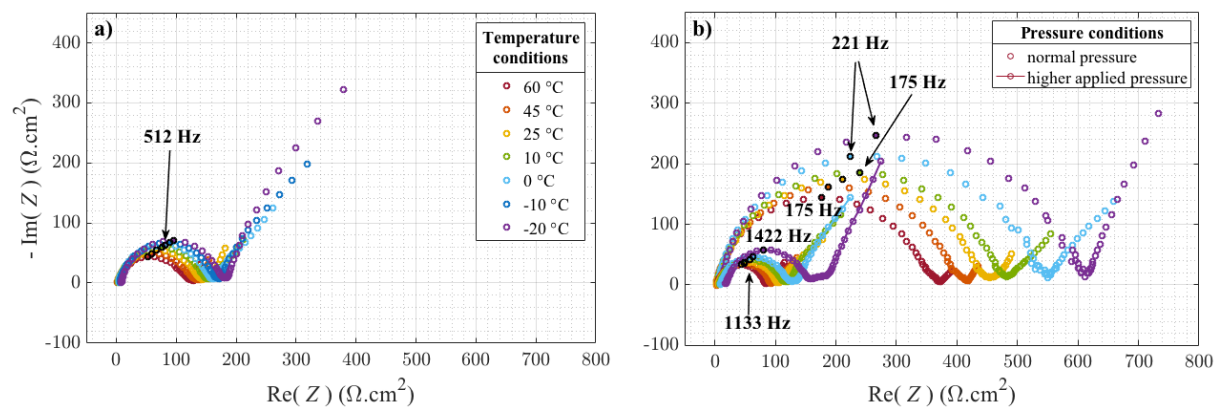
Figure 2 – Impedance spectra of LFP/LFP conventional symmetrical coin cells for different temperatures, at 50% SOC, after 2 formation cycles. Loadings are 15.6 mg cm^{-2} (a) and 19.6 mg cm^{-2} (b). The influence of the applied pressure on the electrodes is also reported in (b).

The normalization of the impedance diagrams with respect to the total active material weight is usually done for characterizing bulk phenomena such as charge transfer. Nevertheless, suspecting that the dominant time-constant is related to a surface contribution, the impedance is preferably

normalized with the geometrical area. The results presented in Figure 2 show that normalized impedance is higher for a higher loading, under normal pressure conditions, even if this pressure should be higher for the thicker electrode. If we ascribe the time-constant to a contact impedance, we have to assume that this contact is worse at higher loading. Indeed, it should be mentioned that some experimental observations support this conclusion. When handling the electrodes before mounting in the coin cell, the differences in mechanical strength can clearly be seen: for higher thickness (*i.e.* higher loading), the electrode material is much more easily removed from the current collector. This can be attributed to heterogeneities in composition along the thickness of the material since carbon black and PVdF tends to diffuse from the collector to the surface during the drying process [24]. The lack of these two components at the electrode/collector interface weakens the adhesion contact. Adhesion and contact are deteriorated at high loading and especially for high drying temperature [24].

The temperature and pressure dependences of the impedance should be taken into account as a function of the physicochemical processes at the interface between the electrode and the current collectors. Temperature dependence is linked to an ionic process in the electrolyte and is associated to a capacitive behavior. Pressure dependence shows a contribution of an electronic process which is attributed to a contact resistance between the LFP particles and the current collector. These variations as a function of the pressure may originate from the porosity of the material. Actually, a tentative model has been proposed by Gaberscek et al. [15] assuming that two types of contacts can be distinguished. On the one hand, LFP active particles are in direct contact with the current collector and on the other hand, electrolyte/collector interface exists within the pore of the electrode.

The impedance in the high frequency domain can be described by an equivalent electrical circuit (EEC) simply composed of a resistor in series with a parallel combination of a second resistance and a constant phase element (*CPE*), as illustrated in Figure 3. The low frequencies part of the spectra is therefore omitted to isolate the contribution of the electrode/collector contact. This can be done since the mass does have a significant contribution only at low frequencies and does not interfere in the LFP/collector contact at high frequencies when this contact is improved by using a coated collector (see below).
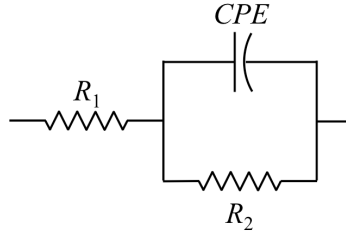
Figure 3 – Equivalent electrical circuit used for the analysis of the high frequency part of the impedance ascribed to the LFP/Al contact.

It is possible to calculate the associated capacitance, by considering a surface distribution time-constant for double-layer, in contrast to a normal distribution [25]. Thus, having the total impedance of the EEC presented in Figure 3, it comes

$$Z(\omega) = R_1 + \frac{R_2}{1 + (j\omega)^\alpha Q R_2} \qquad\qquad Eq.\ 1$$

where ω is the angular frequency, Q and α the coefficient of the *CPE* element. The effective capacitance, C_{eff}, associated to the *CPE* behavior of the electrode thus follows the relation derived by Brug et al. [26]

$$C_{\text{eff}} = Q^{1/\alpha} \left(\frac{R_1 R_2}{R_1 + R_2}\right)^{(1-\alpha)/\alpha} \qquad\qquad Eq.\ 2$$

The values of the *CPE* used to calculate C_{eff} are in the range from 2.2 10^{-6} to 1.0 10^{-5} F$^\alpha$.$\Omega^{\alpha-1}$ and from 0.85 to 0.91 for Q and α, respectively. The value of C_{eff} determined from EIS results is temperature and pressure dependent (Figure 4). The values range between 0.76 - 1.2 µF cm^{-2} at -20 °C and 1.3 - 1.5 µF cm^{-2} at 60 °C. Nonetheless, the double layer capacitance is typically in the range of 10-40 µF cm^{-2}. Moreover, two interfaces exist on the pathway of the charges inside a pore between a particle and the collector: electrolyte/material and electrolyte/collector. Actually, C_{eff} may either be linked to the contact area between the electrolyte and the collector or the contact area between the active material particles and the electrolyte. If we assume that it is the double layer at the LFP particles, the capacitance values need to be scaled by the active area measured by BET. For a developed active area of 5.56 m²/g for the LFP material, the capacitance values range between 0.79 and 1.2 nF cm^{-2} at -20 °C and 1.3 – 1.5 nF cm^{-2} at 60 °C. This is more than four orders of magnitude lower than the typical values encounter for double layer capacitance. This indicates that the measured capacitance is related to the electrolyte/collector interface. The values calculated are still one order of magnitude lower than that of a typical double layer capacitance. However, this overestimation is to be ascribed to that fact that most of the current collector surface is in contact with the active material and the wet surface area of the collector should only account for 10% of the total surface of the collector.

Additionally, the current collector is protected by its native passive film made of alumina (Al_2O_3), formed before mounting the cell (oxygen and moisture), but it is also in contact with a corrosive organic medium. Moisture traces and/or the decomposition of the electrolyte may lead to free protons that react with alumina and dissolve it while also reacting with PF_6^- ions to form HF at the interface, which contributes to convert Al_2O_3 into AlF_3 [27].

Considering the two double layer capacitances $C_{dl,LFP}$ and $C_{dl,Al}$ at the LFP/electrolyte and electrolyte/collector interfaces, respectively, and the capacitance of the passive film C_{film} in series, the effective capacitance C_{eff} (measured during the experiment, at high frequencies) is expressed as

$$\frac{1}{C_{eff}} = \frac{1}{C_{film}} + \frac{1}{C_{dl,LFP}} + \frac{1}{C_{dl,Al}} \qquad\qquad Eq.\ 3$$

The contribution of $C_{dl,LFP}$ can be neglected due to the large surface of the active material leading to a small contribution to C_{eff}. Thus:

$$\frac{1}{C_{eff}} = \frac{1}{C_{film}} + \frac{1}{C_{dl,Al}} \qquad\qquad Eq.\ 4$$

This relation shows that the presence of the thin film adds a capacitive contribution, which can also slightly lower the value of the measured capacitance C_{eff}.

Moreover, the results presented in Figure 4 allows to develop further this approach. When applying a higher pressure to the electrode, the fraction of pores at the electrode/collector interface decreases, which results in a decrease of the free surface at the current collector. Thus, the double layer capacitance is decreased and its contribution lowers the measured effective capacitance C_{eff}, which is experimentally observed on results presented in Figure 4 for both the higher loading (higher internal pressure as the electrode thickness is higher and in a limited space enforced by the coin cell casing) and the higher applied pressure.
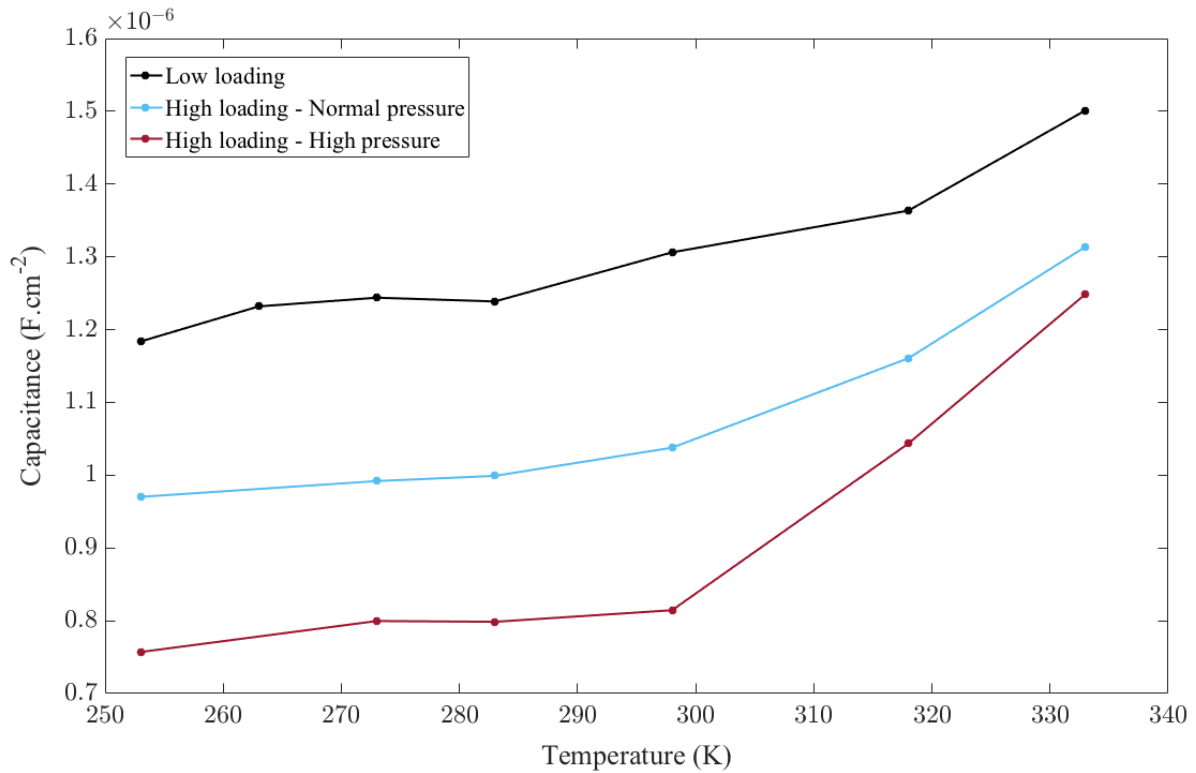
Figure 4 – Capacitance C_{eff} values after fitting the LFP/Al contact time constant with the EEC presented in Fig.3 for different pressure conditions with the capacitance normalized by geometrical surface.

A capacity representation of the impedance data (*i.e.* the Cole-Cole plot) was also used for the capacitance study of the whole behavior of the system. The complex capacitance is obtained from the impedance measurement corrected for the contribution of the electrolyte resistance, R_{e}, and expresses as

$$C(\omega) = \frac{1}{j\omega(Z - R_{\mathrm{e}})} \qquad\qquad Eq.\ 5$$

An example of this representation is shown in Figure 5, for a low loading LFP electrodes. When considering the high frequency domain of the impedance, a *CPE* is observed, which can be described by a series of Voigt elements [28] and which tends towards a pure capacitance at high frequencies (the current flows through the less resistive pathway), as shown by Figure 6. This description allows to obtain the high frequency capacitance independently of the model to be used for explaining the CPE

10
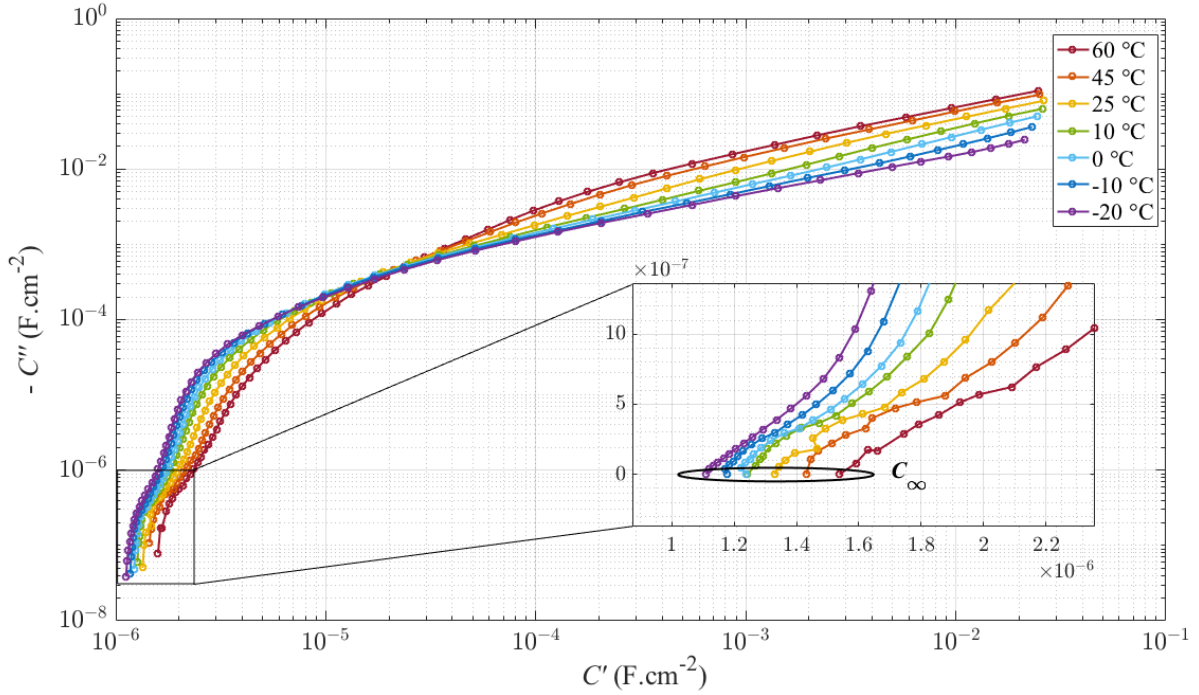
Figure 5 – Cole-Cole representation of the impedance response for LFP-LFP conventional symmetrical coin cell with a low loading as a function of the temperature – calculated from data presented in Fig. 2. Log-log plot for the whole spectrum, linear-linear plot for the zoomed domain.
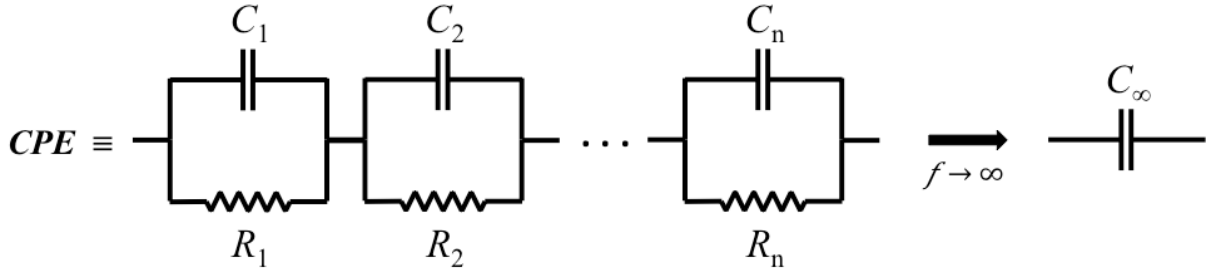
Figure 6 – CPE approximation with Voigt elements showing a pure capacitive behavior (C_∞) at high frequencies

It is then possible to determine the high frequency capacitance C_∞ from the extrapolation of the Cole-Cole plot at $Im(C) = 0$. The values obtained for C_∞ range from 0.53 to 1.54 µF cm-2 for all LFP electrode loadings and for all the temperatures, which is similar to the results obtained with C_{eff}.

The effective capacitance C_{eff} was also determined using a graphical analysis of the variation of the logarithm of the absolute values of the imaginary parts of the impedance as a function of the logarithm of the frequencies. The slope of the curve at high frequencies is attributed to the α parameter of CPE [29]. Then, it is possible to calculate the Q_{eff} from the following the formula

$$Q_{eff} = \sin\left(\frac{\alpha\pi}{2}\right)\frac{-1}{Z_{im}(f)(2\pi f)^\alpha} \qquad\qquad \textit{Eq. 6}$$

The α values obtained vary from 0.75 to 0.98 for all the LFP electrodes thus leading to Q_{eff} values ranging from 5.8 10^{-6} and 1.5 10^{-5} F$^\alpha$ $\Omega^{\alpha-1}$. Then, the effective capacitance C_{eff} is calculated by the Brug formula.

The values of C_{eff} for the three methods are shown in Table 1, for the LFP electrodes with low loading, as an example. There is a good agreement between the fitting method, the Cole-Cole extrapolation and the graphical determination, meaning that the values of C_{eff} is governed by the double layer formed at the current collector. Especially, the Cole-Cole method, which is a direct measurement of the capacitance, is in very good agreement with the use of the Brug formula for converting the *CPE* into a pure capacitance, indicating that the observed contribution follows a surface distribution ascribed to the double layer formed at the electrolyte/collector interface.

Table 1 – Comparison of the capacitance values between C_{eff} and C_∞ for LFP electrodes with low loading as a function of the temperature

Capacitance and method	60 °C	45 °C	25 °C	10 °C	0 °C	-10 °C	-20 °C
C_{eff} (µF cm^{-2}) Brug formula R+(R//CPE) fitting	1.50	1.36	1.31	1.24	1.24	1.23	1.18
C_∞ (µF cm^{-2}) Cole-Cole extrapolation	1.54	1.43	1.33	1.24	1.24	1.18	1.11
C_{eff} (µF cm^{-2}) Graphical determination	1.59	1.47	1.38	1.31	1.26	1.22	1.20

3.2. LFP and ambipolar diffusion

With the conventional two-electrode coin-cell, the impedance response is mainly governed by the electrode/Al contact, which makes it difficult to observe other phenomena, in particular inside the LFP material. Coated current collectors have thus been used to decrease significantly the contact impedance. This study has been performed using the 4-electrode symmetrical cell to enable the tuning of the SOC in situ.

In a first experiment, this new setup has been used with bare Al current collector on which the LFP material was deposited (with a loading of 19.6 mg cm^{-2}). Figure 7a shows that the spectra are very similar in shape but the magnitude of the impedance response is similar to the results obtained for 15.6 mg cm^{-2} LFP electrodes in conventional cells (Figure 2a). Actually, in the 4-electrode setup, the internal pressure is higher due to the addition of elements in the limited volume of the coin cell (extra separators and Li disks), explaining the lower impedance values for the same loading of active LFP material. Moreover, the state of charge has no impact on the

electrode/Al current collector time-constant, as it can be seen in Figure 7b. Thus, the 4-electrode symmetrical setup does not introduce any artifact related to the electrodes morphologies and the spectra are clearly consistent with the expectation for a conventional symmetrical cell.
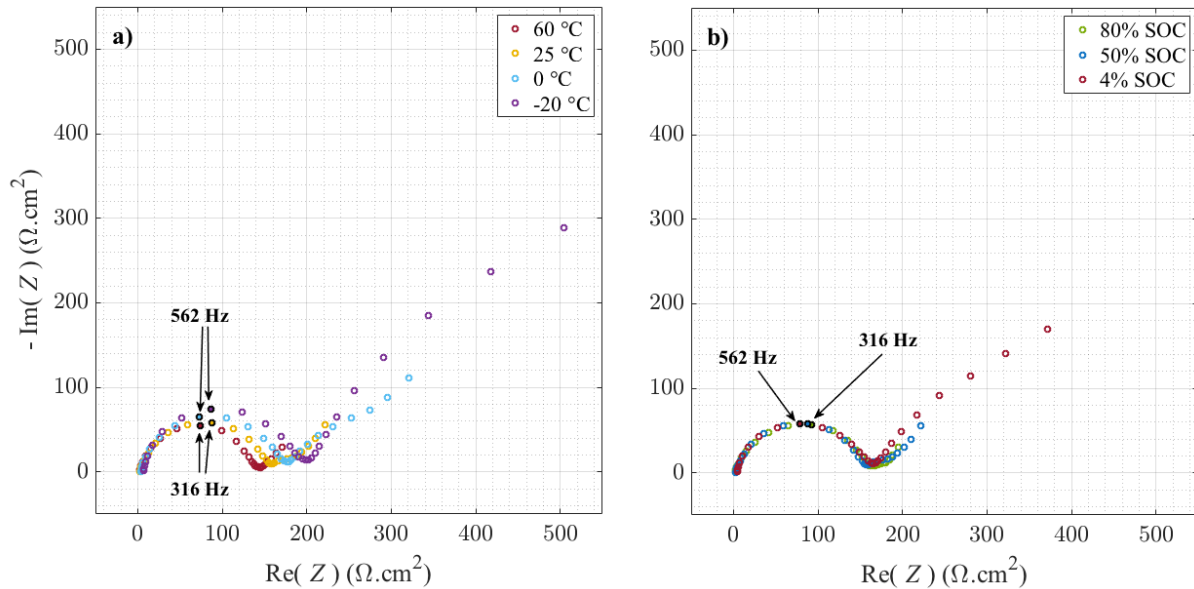
Figure 7 – Impedance spectra for 19.6 mg cm^{-2} LFP/LFP system in 4-electrode symmetrical setup as a function of the temperature at 50% SOC (a) and as a function of the state of charge for measurements at 25 °C (b).

Interestingly, when using LFP electrodes with a coated collector (Figure 8), a significant decrease of the contact contribution in total impedance response is observed. This is partly ascribed to the lower loading of the LFP electrodes on the coated current collector (10 mg cm^{-2} instead of 15.6 mg cm^{-2}), as previously seen (Figure 2). Additionally, the internal pressure in the new setup is also higher which also favors the electrical contact between the active material and the current collector. Figure 9a shows full spectra obtained with the 4-electrode coin-cell and the coated aluminum current collector, which are zoomed (Figure 9b) to better visualize the values of the contact corresponding resistances and the evolution of the associated time-constant. The resistance can be determined from the graphical analysis of the EIS diagrams, and is about 0.80 Ω cm², 1.0 Ω cm² and 4.5 Ω cm² at 60 °C, 25 °C and -20 °C, respectively. These values which thus remain much smaller than those obtained with the conventional cell and current collector. It should also be mentioned that some experiments were performed with these annular electrodes using the conventional setup at different temperature and state of charge (data not shown). Results were in good agreement with those reported in Fig. 8b thus validating the use of this new cell at steady-state for EIS measurements.
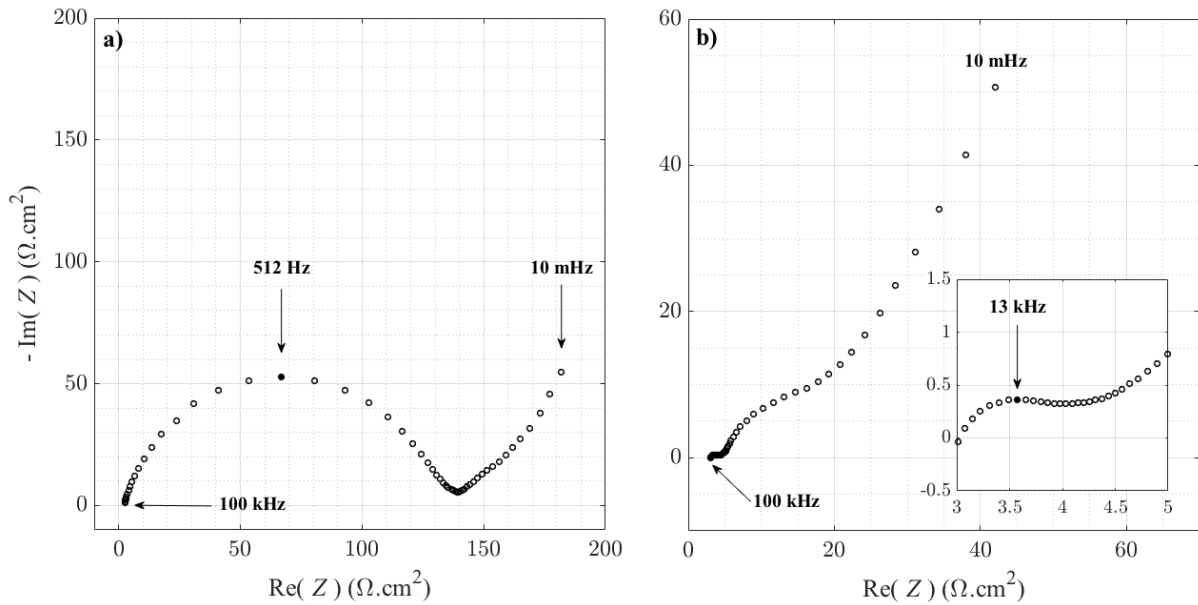
Figure 8 – EIS spectra for LFP/LFP conventional symmetrical coin cell with standard aluminum current collector and a loading of 15.6 mg cm⁻² (a) and for LFP/LFP 4-electrode symmetrical setup with coated aluminum current collector and a loading of 10 mg cm⁻² (b), at 50% SOC at 25°C
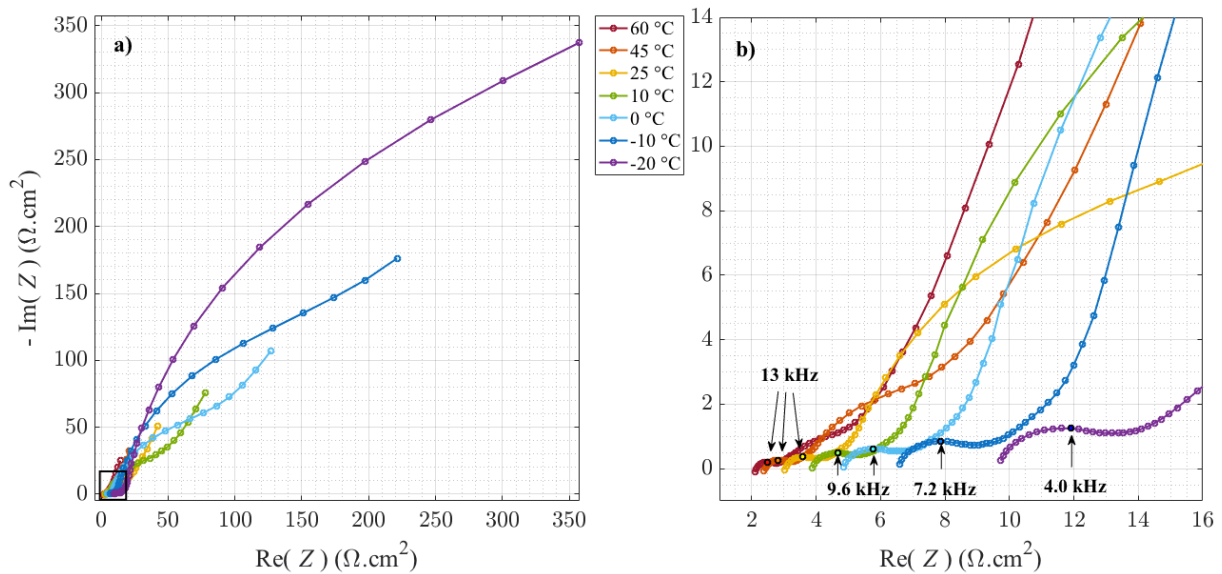
Figure 9 –Full EIS spectra (a) for LFP/LFP 4-electrode symmetrical setup with coated current collector at different measurement temperatures and zoomed window (b) for LFP/collector contact observations, for 50% SOC

It is also important to point out that the 4-electrode symmetrical setup does not dramatically limit the C-rates performances, meaning that it is possible to perform the same battery tests than the ones performed on the conventional setup, at the same low rates (typically C/10 and C/5). Indeed, Figure 10a shows a standard charge/discharge profile of the first formation cycle of the LFP facing Li, at C/10, 60 °C, whereas Figure 10b shows the simultaneous charge/discharge of the two half

cells in the 4-electrode symmetrical setup under the same conditions. The ends of charges and discharges are sharp for both configurations, meaning that all the material has reacted in the lithiation/delithiation processes. The main changes are the slightly inclined plateaus of the $LiFePO_4/FePO_4$ biphasic equilibrium and an extra polarization between the charge and the discharge plateaus (approximately 75 mV for the conventional half-cell and 130 mV for the new setup). The former is directly caused by the curved current lines between the Li electrodes and their facing LFP electrodes, leading to state of charge heterogeneities among LFP particles at this rate (C/10). The latter can be a consequence of the combined effect of the curved current lines and the additional separators used in the new set-up. But the SOC can be homogenized among the LFP particles by increasing the resting time at 60 °C, once the corresponding electrical capacity is reached. It is also worth noting that the lower value of maximum specific capacity for the new 4-electrode set-up (123 mAh/g compared to 158 mAh/g) may originate from the overestimation of the total amount of LFP material in the calculation that could have been removed during the punching steps of the electrodes.
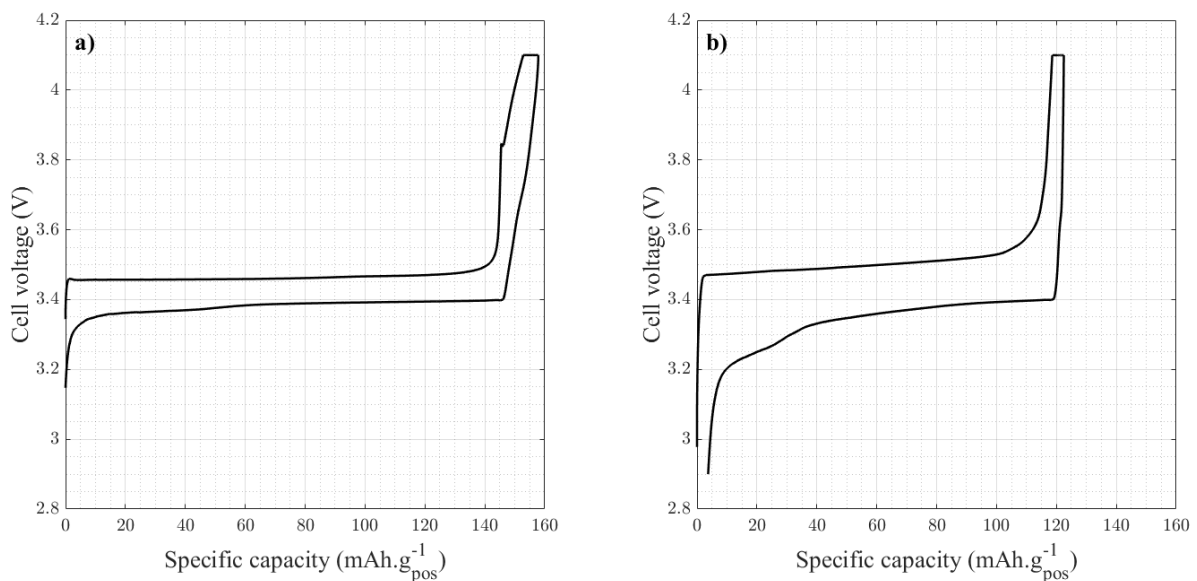
Figure 10 – Charge/discharge profiles of the first formation cycle of LFP vs Li for a conventional half-cell (a) and for the two half-cells in the 4-electrode symmetrical setup (b), at C/10, 60 °C

Interestingly, by greatly improving the contact between the material and the current collector, it is possible to evidence other time-constant corresponding to the intercalation process (Figure 9). Its signature can be seen as the beginning of a semi-circle and is temperature dependent. Moreover, monitoring the SOC of the LFP electrodes shows that the presumed resistance changes with it (Figure 11). For each measurement temperature, the spectra are recorded for blocking

electrodes conditions with 0% and 100% SOC and for intermediate values 25%, 50% and 75% SOC. A global trend can be observed: the higher the SOC, the lower the apparent resistance of this second time constant, except for 0% and 100% where capacitive behavior prevails because all Li sites are full or empty, respectively. The process becomes easier with the increase of the SOC, *i.e.,* the increase of available host sites for Li ions. This time-constant is ascribed to the charge-transfer in the LFP material. The time-constants at lower frequencies are ascribed to diffusion and capacitive properties of the material [30, 31].
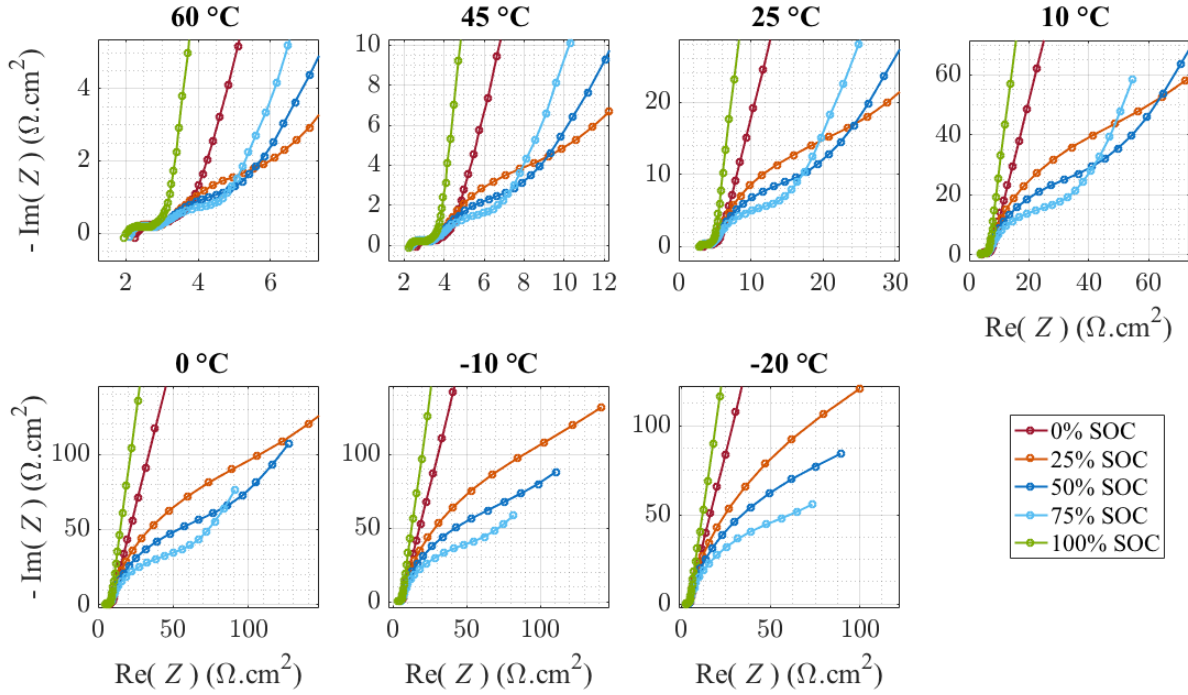
Figure 11 –LFP/LFP impedance response in 4-electrode symmetrical setup as a function of the SOC, with coated aluminum current collector. Each graph corresponds to a different temperature.

Following this assumption, the dependence of the charge transfer resistance as a function of the temperature has been studied. If the current flowing through the electrolyte/LFP interface is thermally activated, it follows an Arrhenius law [32] as

$$i \propto \frac{1}{R_{ct}} = A_0 e^{-E_a/RT} \qquad\qquad Eq.\ 7$$

where R_{ct} is the charge transfer resistance determined from the analysis of the second time-constant of the spectra presented in Figure 11, A_0 is a pre-exponential factor, E_a is the activation energy of the process (in kJ mol^{-1}), R is the gas constant and T the temperature (in K). The resistance can thus be expressed as

$$R_{\text{ct}} = r_0 e^{E_\text{a}/RT} = r_0 e^{\Delta H/kT} \qquad\qquad Eq.\ 8$$

with $R = N_\text{A} \cdot k$ and $\Delta H = \dfrac{E_\text{a}}{N_\text{A}}$

where ΔH is the activation enthalpy (in eV) and N_A is the Avogadro constant.

Three identical LFP/LFP systems with the new coin-cell have been characterized by EIS measurements in the [-20; 60 °C] temperature range and for 0, 25, 50, 75 and 100% SOC. Figure 12 shows the Arrhenius plots for the three cells at the SOC where the time constant is workable, the linear regression and corresponding activation energies.
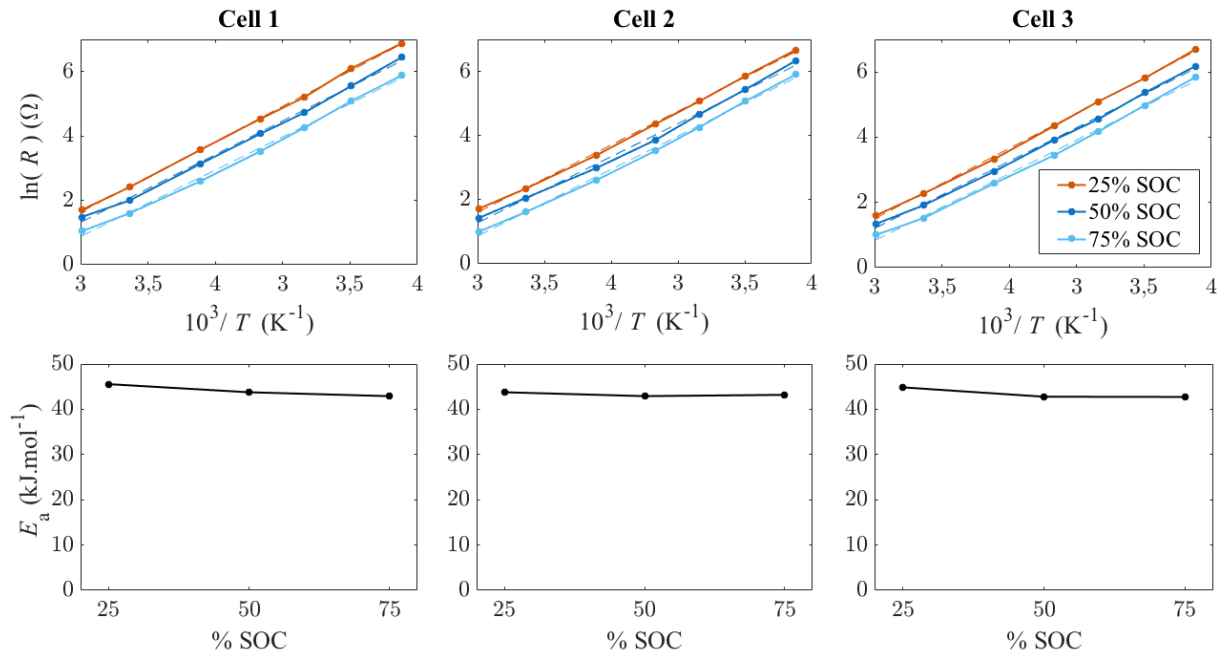
Figure 12 – Arrhenius plots for 3 coin-cells with 4-electrodes symmetrical LFP/LFP setup with linear regression (dashed lines) for 25, 50 and 75% SOC (a) and their corresponding activation energy values (b)

Table 2 – Activation energies and enthalpies determined from linear regression of Arrhenius plot of the charge transfer resistance R_{ct} and the regression coefficient for the three cells as a function of the SOC

	Cell 1			Cell 2			Cell 3		
SOC	**25%**	**50%**	**75%**	**25%**	**50%**	**75%**	**25%**	**50%**	**75%**
Activation energy E_a (kJ mol^{-1})	45.6 ± 0.53	43.8 ± 1.1	42.9 ± 1.1	43.8 ± 0.71	42.9 ± 1.3	43.2 ± 1.0	44.8 ± 0.62	42.8 ± 0.84	42.7 ± 1.2
Activation enthalpy ΔH (eV)	0.472	0.454	0.445	0.454	0.445	0.448	0.465	0.443	0.443

± 5.4	±	±	± 7.3	±	±	± 6.4	± 8.7	±
10^{-3}	0.011	0.012	10^{-3}	0.014	0.010	10^{-3}	10^{-3}	0.012

Table 2 shows the results of the linear fit of the experimental results presented in Figure 12 assuming an Arrhenius law. First, the values for the 3 systems are very similar and a regression coefficient ranging from 0.9956 to 0.9994 was obtained, validating the use of the Arrhenius law for describing the process. The maximum deviation of the activation energies between the three cells is 4.1, 2.3 and 1.2% for 25, 50 and 75% SOC, respectively. Therefore, it is possible to perform accurate EIS measurements on such a symmetrical setup, with good reproducibility from one 4-electrode coin-cell to another. Activation energy values range from 42.7 to 45.6 kJ mol^{-1} (enthalpies from 443 to 472 meV), which is in good agreement with the values obtained in the literature for Li$^+$ charge transfer kinetics at the interface between lithium metal transition metal oxide electrodes such as $Li_{4/3}Ti_{5/3}O_4$ [33], $LiMn_2O_4$ [34] and $LiCoO_2$ [35] and the electrolyte (LiClO$_4$ in EC/DEC or in PC), with 44-48, 50 and 46 kJ mol^{-1}, respectively. Moreover, Li$^+$ charge transfer has been studied between $LiNi_{0.80}Co_{0.15}Al_{0.05}O_2$ electrodes and 1M LiPF$_6$ in EC/DMC/MB/VC mixtures by Jow et al. [32] and an energy of 41 kJ mol^{-1} has been obtained. Indeed, concerning the LFP, the charge transfer phenomenon is assumed to be the diffusion of Li$^+$/e$^-$ polaron, which determines the rate of the electrochemical reaction. The polaronic activation barriers for LFP material are 0.4-0.6 eV [36, 37], with slightly higher values for the fully lithiated state of the particles than the fully delithiated one [38] (determined by Mossbauer spectroscopy: 0.3 and 0.41 eV, respectively). This trend is respected with the values obtained from EIS measurements: the higher the SOC (*i.e.,* the less lithiated LFP particles), the lower activation energy values. Thus, the time-constant observed is attributed to the ambipolar diffusion of the Li$^+$/e$^-$ couple in the LFP particles and a detailed analysis of the spectra allows the activation energy to be determined thanks to the use of the new 4-electrode coin-cell.

4. Conclusions

A new setup of coin cell has been settled which enables to make EIS measurements in a symmetrical configuration, while monitoring the SOC of the electrodes under study, thanks to Li source, in one single coin cell. This greatly improves the reliability of the results since there is no need to dismantle a first source coin cell, extract the electrodes put at a specific SOC and assemble again the 2 electrodes in a conventional symmetrical coin cell. Interestingly, the time saved for performing a study at different SOCs is significant since there is no assembly/disassembly step. Moreover, the rate performances are not drastically degraded, meaning that the change of SOC

can be performed with the same small C-rates as in a conventional 2-electrode configuration. A good reproducibility is to be noticed as well, making the setup reliable to carry the EIS measurements.

The impedance spectrum of LFP has been investigated through both a classical symmetrical setup and a 4-electrode coin-cell.

The importance of having a good electrical contact between the aluminum current collector and the electrode material was pointed out as a stray contribution on the impedance response (in the high frequency domain) hinders the signal of interest for studying battery performances. Interestingly, the use of a carbon coating onto the collector greatly improves the contact and reduces its impedance. A detailed analysis of the impedance response of the battery thus show that the rate-limiting step is the Li^+/e^- diffusion during the electrochemical reaction between the lithiated phase $LiFePO_4$ and the delithiated one $FePO_4$. Indeed, its activation barrier has an energy of about 44-45 kJ mol^{-1}, 43-44 kJ mol^{-1} and 43 kJ mol^{-1} for 25, 50 and 75% SOC, respectively, which is in good agreement with the polaron diffusion in LFP particles.

1. Srinivasan V, Newman J (2004) Discharge Model for the Lithium Iron-Phosphate Electrode. Journal of The Electrochemical Society 151:A1517-A29

2. MacNeil DD, Lu Z, Chen Z, Dahn JR. A comparison of the electrode/electrolyte reaction at elevated temperatures for various Li-ion battery cathodes. 2002.

3. Takahashi M, Tobishima S-i, Takei K, Sakurai Y. Reaction behavior of LiFePO4 as a cathode material for rechargeable lithium batteries. 2002.

4. Padhi AK, Nanjundaswamy KS, Goodenough JB (1997) Phospho-olivines as Positive-Electrode Materials for Rechargeable Lithium Batteries. Journal of The Electrochemical Society 144:1188-94

5. Wang C, Hong J (2007) Ionic/Electronic Conducting Characteristics of LiFePO4 Cathode Materials: The Determining Factors for High Rate Performance. Electrochemical and Solid-State Letters 10:A65-A9

6. Amine K, Liu J, Belharouak I (2005) High-temperature storage and cycling of C-LiFePO4/graphite Li-ion cells. Electrochemistry Communications 7:669-73

7. Yang W, Wang Z, Chen L, Chen Y, Zhang L, Lin Y, et al. (2017) Suppression of degradation for lithium iron phosphate cylindrical batteries by nano silicon surface modification. RSC Advances 7:33680-7

8. Takahara H, Miyauchi H, Tabuchi M, Nakamura T. Elemental Distribution Analysis of LiFePO4/Graphite Cells Studied with Glow Discharge Optical Emission Spectroscopy (GD-OES). 2012.

9. Striebel K, Shim J, Sierra A, Yang H, Song X, Kostecki R, et al. (2005) The development of low cost LiFePO4-based high power lithium-ion batteries. Journal of Power Sources 146:33-8

10. Zheng Y, He Y-B, Qian K, Li B, Wang X, Li J, et al. (2015) Deterioration of lithium iron phosphate/graphite power batteries under high-rate discharge cycling. Electrochimica Acta 176:270-9

11. Li D, L. Danilov D, Gao L, Yang Y, Notten PHL (2016) Degradation Mechanisms of C6/LiFePO4 Batteries: Experimental Analyses of Cycling-induced Aging. Electrochimica Acta 210:445-55

12. Li D, Danilov DL, Gao L, Yang Y, Notten PHL (2016) Degradation Mechanisms of the Graphite Electrode in C6/LiFePO4 Batteries Unraveled by a Non-Destructive Approach. Journal of The Electrochemical Society 163:A3016-A21

13. Eliseeva SN, Apraksin RV, Tolstopjatova EG, Kondratiev VV (2017) Electrochemical impedance spectroscopy characterization of LiFePO4 cathode material with carboxymethylcellulose and poly-3,4-ethylendioxythiophene/polystyrene sulfonate. Electrochimica Acta 227:357-66

14. Shi J-Y, Yi C-W, Kim K (2010) An Investigation of LiFePO 4 /Poly(3,4-ethylenedioxythiophene) Composite Cathode Materials for Lithium-Ion Batteries. Bulletin of the Korean Chemical Society 31:2698-700

15. Gaberscek M, Moskon J, Erjavec B, Dominko R, Jamnik J (2008) The Importance of Interphase Contacts in Li Ion Electrodes: The Meaning of the High-Frequency Impedance Arc. Electrochemical and Solid-State Letters 11:A170-A4

16. Ender M, Illig J, Ivers-Tiffée E (2017) Three-Electrode Setups for Lithium-Ion Batteries: I. Fem-Simulation of Different Reference Electrode Designs and Their Implications for Half-Cell Impedance Spectra. Journal of The Electrochemical Society 164:A71-A9

17. Costard J, Ender M, Weiss M, Ivers-Tiffée E (2017) Three-Electrode Setups for Lithium-Ion Batteries: II. Experimental Study of Different Reference Electrode Designs and Their Implications for Half-Cell Impedance Spectra. Journal of The Electrochemical Society 164:A80-A7

18. Waldmann T, Hogg B-I, Wohlfahrt-Mehrens M (2018) Li plating as unwanted side reaction in commercial Li-ion cells – A review. J Power Sources 384:107-24

19. Li Y, Han X, Feng X, Chu Z, Gao X, Li R, et al. (2021) Errors in the reference electrode measurements in real lithium-ion batteries. J Power Sources 481

20. Chu Z, Feng X, Liaw B, Li Y, Lu L, Li J, et al. (2018) Testing Lithium-Ion Battery with the Internal Reference Electrode: An Insight into the Blocking Effect. J Electrochem Soc 165:A3240-A8

21. Hoshi Y, Narita Y, Honda K, Ohtaki T, Shitanda I, Itagaki M (2015) Optimization of reference electrode position in a three-electrode cell for impedance measurements in lithium-ion rechargeable battery by finite element method. J Power Sources 288:168-75

22. Raijmakers LHJ, Lammers MJG, Notten PHL (2018) A new method to compensate impedance artefacts for Li-ion batteries with integrated micro-reference electrodes. Electrochim Acta 259:517-33

23. Solchenbach S, Pritzl D, Kong EJY, Landesfeind J, Gasteiger HA (2016) A Gold Micro-Reference Electrode for Impedance and Potential Measurements in Lithium Ion Batteries. Journal of The Electrochemical Society 163:A2265-A72

24. Stein M, Mistry A, Mukherjee PP (2017) Mechanistic Understanding of the Role of Evaporation in Electrode Processing. Journal of The Electrochemical Society 164:A1616-A27

25. Hirschorn B, Orazem ME, Tribollet B, Vivier V, Frateur I, Musiani M (2010) Determination of effective capacitance and film thickness from constant-phase-element parameters. Electrochimica Acta 55:6218-27

26. Brug GJ, van den Eeden ALG, Sluyters-Rehbach M, Sluyters JH (1984) The analysis of electrode impedances complicated by the presence of a constant phase element. Journal of Electroanalytical Chemistry and Interfacial Electrochemistry 176:275-95

27. Ma T, Xu G-L, Li Y, Wang L, He X, Zheng J, et al. (2017) Revisiting the Corrosion of the Aluminum Current Collector in Lithium-Ion Batteries. The Journal of Physical Chemistry Letters 8:1072-7

28. Agarwal P, Orazem ME, Garcia-Rubio LH (1992) Measurement Models for Electrochemical Impedance Spectroscopy: I . Demonstration of Applicability. Journal of The Electrochemical Society 139:1917-27

29. Orazem ME, Pébère N, Tribollet B (2006) Enhanced Graphical Representation of Electrochemical Impedance Data. Journal of The Electrochemical Society 153:B129-B36

30. Ho C, Raistrick ID, Huggins RA (1980) Application of A-C Techniques to the Study of Lithium Diffusion in Tungsten Trioxide Thin Films. J Electrochem Soc 127:343-50

31. Barral G, Diard JP, Montella C (1984) Etude d'un modele de reaction electrochimique d'insertion—I. Resolution pour une commande dynamique a petit signal. Electrochim Acta 29:239-46

32. Jow TR, Allen J, Marx M, Nechev K, Deveney B, Rickman S (2010) Electrolytes, SEI and charge discharge kinetics in Li-ion batteries. ECS Transactions 25:3-12

33. Doi T, Iriyama Y, Abe T, Ogumi Z (2005) Pulse Voltammetric and ac Impedance Spectroscopic Studies on Lithium Ion Transfer at an Electrolyte/Li4/3Ti5/3O4 Electrode Interface. Analytical Chemistry 77:1696-700

34. Yamada I, Abe T, Iriyama Y, Ogumi Z (2003) Lithium-ion transfer at LiMn2O4 thin film electrode prepared by pulsed laser deposition. Electrochemistry Communications 5:502-5

35. Yamada I, Iriyama Y, Abe T, Ogumi Z (2007) Lithium-ion transfer on a LixCoO2 thin film electrode prepared by pulsed laser deposition—Effect of orientation. Journal of Power Sources 172:933-7

36. Delacourt C, Laffont L, Bouchet R, Wurm C, Leriche J-B, Morcrette M, et al. (2005) Toward Understanding of Electrical Limitations (Electronic, Ionic) in LiMPO4 (M = Fe , Mn) Electrode Materials. Journal of The Electrochemical Society 152:A913-A21

37. Malik R, Abdellahi A, Ceder G (2013) A Critical Review of the Li Insertion Mechanisms in LiFePO4 Electrodes. Journal of The Electrochemical Society 160:A3179-A97

38. Tan H, Fultz B (2011) Rapid Electron Dynamics at Fe Atoms in Nanocrystalline Li0.5FePO4 Studied by Mössbauer Spectrometry. The Journal of Physical Chemistry C 115:7787-92